Regioselective Protonation of the η^4-Anthracene Ligand in $[Mn(\eta^4\text{-}C_{14}H_{10})(CO)_3]^-$ To Give an η^5-Anthracenyl Complex $[Mn(\eta^5\text{-}C_{14}H_{11})(CO)_3]$ That Undergoes a Low-Energy 1,4-Hydride Exchange Reaction

Jacqueline M. Veauthier,[†] Albert Chow,[‡] Gideon Fraenkel,*[,‡] Steven J. Geib,*[,†] and N. John Cooper*[,†]

Departments of Chemistry, University of Pittsburgh, Pittsburgh, Pennsylvania 15260, and Ohio State University, Columbus, Ohio 43210

Received September 20, 1999

Protonation of the terminal (η^4-anthracene) manganese tricarbonyl anion $[Mn(\eta^4\text{-}C_{14}H_{10})(CO)_3]^-$ gives the terminal (η^5-anthracenyl) manganese tricarbonyl complex $[Mn(\eta^5\text{-}C_{14}H_{11})(CO)_3]$. Single-crystal X-ray diffraction analysis confirms that the proton adds to the hydrocarbon ring, and labeling studies indicate that protonation is regiospecific and occurs at the endo site. Magnetization transfer experiments establish rapid spin population transfer from the exo site to the para ring position. This is proposed to involve an intermediate metal hydride, and dynamic NMR studies have been used to determine that the free energy barrier to this exchange is ca. 14.5 kcal/mol at and below ambient temperatures. This is interpreted in terms of a modification of the mechanism of Lamanna and Brookhart for the isomerization within 6-*exo*-^{1}H-$[Mn(\eta^5\text{-}C_6HD_5)(CO)_3]$.

Introduction

Recent work from our group[1−4] and others[5−7] has established that arenes can be activated by coordination to highly reduced metal centers. The arenes are most typically mononuclear arenes like benzene, and in the activated form the arenes are bound to the metal center in a mode in which the arene does not adopt the familiar, planar, π-coordination geometry in which all the arene atoms involved in the π-bonding network bond to the metal center; the arenes are forced instead into a reduced hapticity bonding mode (η^4 or η^2), and the locus of reactivity is then on the arene because of the loss of aromaticity in the lower hapticity coordination state.

A few examples are known in which polyaromatic hydrocarbons are also activated through reduced hapticity coordination, but examples to date are limited to naphthalene ligands[2,5,6b,c] and an Os(II) compound of anthracene.[5a] Our recent observation that the η^4-anthracene complex $[Mn(\eta^4\text{-}C_{14}H_{10})(CO)_3]^-$ (**1**$^-$) can be formed by substitution of anthracene for benzene in $[Mn(\eta^4\text{-}C_6H_6)(CO)_3]^-$ (Scheme 1)[4] potentially offers a broad approach to reductively activated polyaromatic hydrocarbons and has led us to investigate the reactivity of **1**$^-$ with electrophiles.

The thermodynamic reduction product of anthracene, 9,10-dihydroanthracene, forms as a result of dihydrogen addition to the middle ring of anthracene, but with the anthracene ligand bound terminally to the metal in **1**$^-$ protonation should occur at the end ring. We now wish to report that this is indeed the case and that protonation gives the η^5-anthracenyl complex $[Mn(\eta^5\text{-}C_{14}H_{11})(CO)_3]$ (**2**), but that formation of the new C−H bond is readily reversible and that **2** is fluxional through a rapid metal-mediated 1,4-hydride migration. There is no evidence in the structural data for any unusual ground-state interaction between the endo C−H and the metal center. While this work was in progress, an analogous 1,4-hydride shift within $[Mn(\eta^5\text{-}C_{10}H_9)(CO)_3]$ was reported by Georg and Kreiter.[8]

Experimental Section

General Procedures. All reactions and manipulations were carried out under an atmosphere of dry, oxygen-free nitrogen by means of standard Schlenk techniques or a Vacuum Atmospheres drybox unless otherwise stated. Glassware was soaked in KOH-saturated 2-propanol for ca. 12 h and rinsed with water and acetone before it was dried. Glass reaction vessels were oven-dried and flamed under vacuum before use. Krytox fluorinated grease was used for all glass joints unless otherwise stated.

[†] University of Pittsburgh.
[‡] Ohio State University.

(1) (a) Leong, V. S.; Cooper, N. J. *J. Am. Chem. Soc.* **1988**, *110*, 2644, and references therein. (b) Corella, J. A.; Cooper, N. J. *J. Am. Chem. Soc.* **1990**, *112*, 2832.
(2) (a) Leong, V. S.; Cooper, N. J. *Organometallics* **1988**, *7*, 2058. (b) Thompson, R. L.; Lee, S.; Rheingold, A. L.; Cooper, N. J. *Organometallics* **1991**, *10*, 1657.
(3) (a) Thompson, R. L.; Geib, S. J.; Cooper, N. J. *J. Am. Chem. Soc.* **1991**, *113*, 8961. (b) Lee, S. J.; Cooper, N. J. *J. Am. Chem. Soc.* **1991**, *113*, 716.
(4) (a) Lee, S.; Geib, S. J.; Cooper, N. J. *J. Am. Chem. Soc.* **1995**, *117*, 9572. (b) Lee, S. Ph.D. Thesis, University of Pittsburgh, 1992.
(5) (a) Harman, W. D. *Chem. Rev.* **1997**, *97*, 1953. (b) Winemiller, M. D.; Harman, W. D. *J. Am. Chem. Soc.* **1998**, *120*, 7835.
(6) (a) Rieke, R. D.; Daruwala, K. P.; Schulte, L. D.; Pankas, S. M. *Organometallics*, **1992**, *11*, 284. (b) Henry, W. P.; Rieke, R. D. *J. Am. Chem. Soc.* **1983**, *105*, 6314. (c) Rieke, R. D.; Henry, W. P.; Arney, J. S. *Inorg. Chem.* **1987**, *26*, 420.
(7) Son, S. U.; Lee, S. S.; Chung, Y. K. *J. Am. Chem. Soc.* **1997**, *119*, 7711.
(8) Georg, A.; Kreiter, C. G. *Eur J. Inorg. Chem.* **1999**, 651.

10.1021/om990735g CCC: $19.00
Publication on Web 01/26/2000

Scheme 1

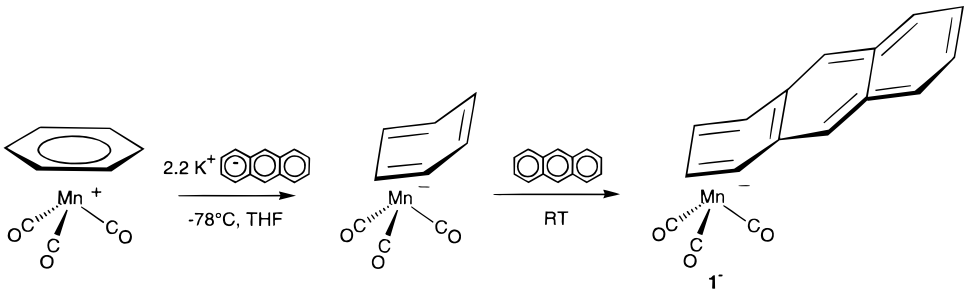

Air sensitive filtrations were performed using positive nitrogen pressure to force solutions through a specially constructed filtration cannula. This was made by fitting the port end of a stainless steel cannula with a piece of hardened filter paper (Whatman's No. 5 and glass microfiber were used separately or layered) and then securing it with Teflon tape. The port of the cannula was made by welding a stainless steel filter support to one end of the cannula (Popper).

Solutions were stirred magnetically. A bath temperature of −78 °C was maintained with dry ice in acetone.

All solvents were freshly distilled under nitrogen before use. Tetrahydrofuran (THF) and diethyl ether (Et_2O) were predried over sodium ribbon. THF was distilled from potassium, and Et_2O was distilled from sodium/benzophenone ketyl. Methylene chloride (CH_2Cl_2) was freshly distilled from CaH_2. Benzene (C_6H_6) was distilled from sodium. *n*-Pentane (C_5H_{12}) was stirred over concentrated H_2SO_4 for more than 24 h, neutralized with K_2CO_3, and distilled from CaH_2. All deuterated NMR solvents were purchased from Cambridge Isotope Labs and used as received.

Unless otherwise stated, all reagents were used as received. Manganese carbonyl [$Mn_2(CO)_{10}$] was purchased from Strem Chemicals Inc. Aqueous hexafluorophosphoric acid (HPF_6), trifluoroacetic acid (CF_3CO_2H(D)), anthracene ($C_{14}H_{10}$), and bis(triphenylphosphoranylidene)ammonium chloride ([PPN]Cl) were purchased from Aldrich. Aluminum chloride ($AlCl_3$) was purchased from EM Science.

Potassium anthracenide [$K(C_{14}H_{10})$] was prepared by dissolving freshly cut potassium metal (Aldrich) in a solution of anthracene (1.5 equiv) in THF and stirring 8 h under a nitrogen atmosphere at room temperature. Potassium anthracenide solutions were stored under nitrogen in Suba-sealed Schlenk vessels at −70 °C.

Preparation of [Mn(η^6-C_6H_6)$(CO)_3$]PF_6. Samples of [Mn(η^6-C_6H_6)$(CO)_3$]PF_6 were prepared by a variation of the method described by Wilkinson and co-workers.[9] In a typical reaction, a mixture of 5.63 g (24.4 mmol) of [$Mn(CO)_5Cl$] and 4.50 g (33.7 mmol) of $AlCl_3$ dissolved in 52.0 mL of anhydrous C_6H_6 was refluxed for 9 h. The reaction flask was quenched with 100 mL of ice water to give an upper organic layer and lower aqueous phase. A separatory funnel was used to collect the lower aqueous phase that was washed with 3 × 50 mL of pentane (or until the pentane layer became clear), while the upper organic layer was discarded. The clean yellow aqueous solution was treated with excess cold aqueous HPF_6 to precipitate a pale yellow powder. This was collected on a medium Büchner filter frit, washed with H_2O, methanol, and Et_2O, and then dried under vacuum to yield 6.39 g (17.7 mmol, 72%) of [Mn(η^6-C_6H_6)$(CO)_3$]PF_6: IR ($\nu_{C\equiv O}$ only, Nujol) 2090 (s), 2020 (s, br) cm^{-1}; ^1H NMR (300 MHz, CD_3CN) δ 6.48 (s, 6H, Ph).

Infrared spectra were recorded on a Perkin-Elmer model 783 spectrophotometer. Solution spectra were recorded with samples in Teflon-sealed solution cells fit with Suba Seal septa and thoroughly purged with nitrogen before use. All infrared spectra of samples taken from solutions at specified temperatures were recorded at room temperature. Polystyrene was used as the external standard (1601 cm^{-1} peak). ^1H NMR spectra were recorded on a Bruker AC 300 spectrometer at 300 MHz. ^{13}C NMR spectra were recorded on a Bruker AC 300 at 75 MHz. ^2H NMR spectra were recorded on a Bruker DPX-300 NMR spectrometer at 46 MHz. $^1H-^1H$ COSY and $^1H-^1H$ NOESY NMR spectra were recorded on a Bruker DPX-300 NMR spectrometer at 300 MHz. Mass spectra were recorded on a JEOL-SX102A mass spectrometer. Peaks are reported in units of mass per charge (*m*/*e*) as percentages of the base peak.

Dynamic NMR. Variable temperature was achieved by replacing the normal air stream to the Bruker Aspect 3000 with a stream of nitrogen gas. The gas was passed from a 20 L Dewar of liquid nitrogen through a Dewared Pyrex glass tube. The gas was heated as needed as determined by a thermocouple on the insert wall below the receiver coil. Temperatures within the NMR probe were calibrated against methanol and found to be accurate to within 0.2 °C. Samples for variable-temperature NMR were prepared in $C_6D_6CD_3$ in 5 mm NMR tubes, degassed by several freeze/pump/thaw cycles, and then sealed under vacuum.

Population transfer studies were carried out by selectively saturating one resonance peak at a time and then applying a nonselective $\pi/2$ observation pulse to record the spectrum. Pulse widths of π and $\pi/2$ were measured for each temperature and were determined by obtaining a well-phased Fourier-transformed FID at low power and then adjusting the pulse width setting several times to observe the Fourier-transformed FID (using the same phase angle as that used at low power) which is exactly π out of phase as the π pulse width. The $\pi/2$ pulse width is then one-half the width of the π pulse.

X-ray Crystallography. Crystals for X-ray diffraction studies were coated with fluorolube, then mounted on a glass fiber and coated with epoxy. X-ray data were collected on a Siemens P3 diffractometer using graphite-monochromatized Mo Kα radiation ($\lambda = 0.71073$ Å). Data processing and graphics were done with the Siemens SHELXTL package program. All non-hydrogen atoms were located and refined anisotropically. All hydrogen atoms in [Mn(η^5-$C_{14}H_{11}$)$(CO)_3$] were located and refined isotropically, and all hydrogen atoms in [PPN][Mn(η^4-$C_{14}H_{10}$)$(CO)_3$] were calculated and placed in idealized positions ($d_{C-H} = 0.96$ Å).

Microanalysis. Microanalyses were performed by Atlantic Microlab, Norcross, GA.

Reaction of [Mn(η^6-C_6H_6)$(CO)_3$]PF_6 with K($C_{14}H_{10}$) and Isolation of [PPN][Mn(η^4-$C_{14}H_{10}$)$(CO)_3$]. A fast addition (<5 s) of 2.2 equiv of K($C_{14}H_{10}$) to a slurry of 0.601 g (1.66 mmol) of [Mn(η^6-C_6H_6)$(CO)_3$]PF_6 in THF at −78 °C resulted in an immediate change from a yellow slurry to an orange-brown solution and finally to a orange-brown slurry. IR spectra of a sample removed from the orange-brown slurry showed consumption of the starting material and the appearance of new $\nu_{C\equiv O}$ bands (IR, THF: 1940 (s), 1845 (s), and 1820 (s) cm^{-1}) assigned to [Mn(η^4-C_6H_6)$(CO)_3$]K. The slurry dissolved near −42 °C. The solution was allowed to warm to room temperature and was stirred overnight. Solid [PPN]Cl (0.810 g, 1.41

(9) Winkhaus, G.; Pratt, L.; Wilkinson, G. *J. Chem. Soc.* **1961**, 3807.

mmol) was added and stirred at room temperature for 3 h. The solvent was removed, and the orange-brown powder was redissolved in CH_2Cl_2 and filtered via cannula to give a clear dark orange solution, which was concentrated and layered with Et_2O (1:3, CH_2Cl_2/Et_2O) to give large orange crystals of [PPN][Mn(η^4-$C_{14}H_{10}$)$(CO)_3$] (1.17 mmol, 70.5%): IR ($\nu_{C\equiv O}$ only, THF) 1940 (s), 1845 (s), 1820 (s) cm^{-1}; IR ($\nu_{C\equiv O}$ only, CH_2Cl_2) 1945 (s), 1850 (s), 1825 (s) cm^{-1}; ^1H NMR (300 MHz, CD_2Cl_2) δ 7.07 (dd, $J_{5-4} = 6.05$ Hz, $J_{5-4'} = 3.31$ Hz, 2H, $H_{5,5'}$), 6.86 (dd, $J_{4-5} = 6.05$ Hz, $J_{4-5'} = 3.31$ Hz, 2H, $H_{4,4'}$), 6.34 (s, 2H, $H_{3,3'}$), 5.62 (dd, $J_{2-1} = 4.91$ Hz, $J_{2-1'} = 2.80$ Hz, 2H, $H_{2,2'}$), 2.79 (dd, $J_{1-2} = 4.91$ Hz, $J_{1-2'} = 2.80$ Hz, 2H, $H_{1,1'}$). Anal. Calcd for $C_{53}H_{40}MnNO_3P_2$: C, 74.39; H, 4.71; N, 1.64. Found: C, 74.47; H, 4.77; N, 1.63.

Reaction of K[Mn(η^4-$C_{14}H_{10}$)$(CO)_3$] with CF_3CO_2H. A fast addition of 2.0 equiv of K($C_{14}H_{10}$) to a slurry of 0.200 g (0.553 mmol) of [Mn(η^6-C_6H_6)$(CO)_3$]PF_6 in THF at −78 °C resulted in a change from a yellow slurry to an orange-brown solution and finally to an orange-brown slurry. IR spectra of a sample removed from the orange-brown slurry showed consumption of the starting material and the appearance of new $\nu_{C\equiv O}$ bands (IR, THF: 1940 (s), 1845 (s), 1820 (s) cm^{-1}) assigned to [Mn(η^4-C_6H_6)$(CO)_3$]K. The slurry dissolved near −42 °C. The solution was allowed to warm to room temperature and was stirred overnight to give [Mn(η^4-$C_{14}H_{10}$)$(CO)_3$]K. Addition of 43 mL (0.558 mmol) of CF_3CO_2H resulted in an immediate color change from orange to dark red. IR spectra of the red solution showed the presence of a neutral complex (IR: $\nu_{C\equiv O}$, THF, 2010 (s), 1928 (s), 1915 (s) cm^{-1}). There was also a band at 1695 (m) cm^{-1} assigned to [PPN][CF_3CO_2]. The solvent was removed, and the red-brown powder was redissolved in *n*-pentane and filtered via cannula to give a dark red solution. Wine-red microcrystals of [Mn(η^5-$C_{14}H_{11}$)$(CO)_3$] (65% spectroscopic yield) were obtained by slowly cooling the concentrated pentane solution to −20 °C.

Reaction of [PPN][Mn(η^4-$C_{14}H_{10}$)$(CO)_3$] with CF_3CO_2H and Isolation of [Mn(η^5-$C_{14}H_{11}$)$(CO)_3$]. To a slurry of 0.198 g (0.232 mmol) of [PPN][Mn(η^4-$C_{14}H_{10}$)$(CO)_3$] in 20 mL of *n*-pentane was added 17.9 mL (0.232 mmol) of CF_3CO_2H. A dark red pentane solution formed, while much of the yellow [PPN][Mn(η^4-$C_{14}H_{10}$)$(CO)_3$] remained behind. The red pentane solution was filtered, and subsequent treatments of the yellow solid in pentane with CF_3CO_2H continued to give red solutions that were collected by filtration. IR spectra of the red solution confirmed the presence of a neutral complex (IR: $\nu_{C\equiv O}$, pentane, 2020 (vs), 1942 (vs), 1925 (vs) cm^{-1}). The infrared spectrum also contained a band at 1700 (m) cm^{-1} assigned to [PPN][CF_3CO_2], which is sparingly soluble in pentane and Et_2O. Slow cooling of the pentane solution to −20 °C gave 0.047 g of small X-ray quality wine-red crystals of [Mn(η^5-$C_{14}H_{11}$)$(CO)_3$] (0.148 mmol, 38%): ^1H NMR (300 MHz, $C_6D_5CD_3$, 257 K) δ 7.35 (d, $J_{8-9} = 8.23$ Hz, 1H, H_8), 7.31 (s, 1H, H_6), 7.17 (d, $J_{11-10} = 8.23$ Hz, 1H, H_{11}), 6.96 (dt, 2H, $H_{9,10}$), 6.84 (s, 1H, H_{13}), 6.06 (d, $J_{4-3} = 5.6$ Hz, 1H, H_4), 4.96 (t, $J_{3-4}/J_{3-2} = 6.4$ Hz, 1H, H_3), 3.32 (td, $J_{2-3}/J_{2-1endo} = 5.9$ Hz, 1H, H_2), 2.84 (dd, $J_{1endo-1exo} = 15.4$ Hz, $J_{1endo-2} = 4.9$ Hz, 1H, H_{endo}), 2.66 (d, $J_{1exo-1endo} = 15.4$ Hz, 1H, H_{exo}); ^{13}C NMR (75 MHz, $C_6D_5CD_3$, 257 K) δ 224 (s(br), 3C, C≡O), 125−135 (8C, C_{6-13}), 108 (s, 1C, C_5), 106 (s, 1C, C_{14}), 96.6 (d, $J_{C4-H4} = 168$ Hz, 1C, C_4), 74.9 (d, $J_{C3-H3} = 176$ Hz, 1C, C_3), 50.4 (d, $J_{C2-H2} = 166$ Hz, 1C, C_2), 30.0 (t, $J_{C1-Hexo} \sim J_{C1-Hendo} = 130$ Hz, 1C, C_1); $^1H-^1H$ NOESY NMR (300 MHz, $C_6D_5CD_3$, 257 K) large correlation for δ 7.31 and 6.06 (H_6 and H_4), small correlation for δ 6.84 and 6.06 (H_{13} and H_4); mass spectrum (EI) *m/z* 318 (5.9), 290 (25.0), 262 (17.9), 234 (53.0), 179 (100), 152 (17.0), 97 (6.0), 83 (7.9), 69 (13.0), 55 (26.8). Anal. Calcd for $C_{17}H_{11}MnO_3$: C, 64.17; H, 3.48. Found: C, 63.24; H, 3.58.

Reaction of [PPN][Mn(η^4-$C_{14}H_{10}$)$(CO)_3$] with CF_3CO_2D and Isolation of [Mn(η^5-$C_{14}H_{10}$D)$(CO)_3$]. To a slurry of 0.479 g (0.560 mmol) of [PPN][Mn(η^4-$C_{14}H_{10}$)$(CO)_3$] in 25 mL of *n*-pentane was added 43.0 mL (0.558 mmol) of CF_3CO_2D. A dark red pentane solution formed, while much of the yellow [PPN][Mn(η^4-$C_{14}H_{10}$)$(CO)_3$] remained behind. The red pentane solution was filtered. IR spectra of the red solution showed the presence of a neutral complex (IR: $\nu_{C\equiv O}$, pentane, 2020 (vs), 1942 (vs), 1925 (vs) cm^{-1}). There was also a band at 1700 (m) cm^{-1} assigned to [PPN][CF_3CO_2]). Slow cooling of the pentane solution to −20 °C gave small wine-red crystals of [Mn(η^5-$C_{14}H_{10}$D)$(CO)_3$] (0.236 mmol, 42%): ^1H NMR (300 MHz, $C_6D_5CD_3$, 257 K) δ 7.35 (d, $J_{8-9} = 8.25$ Hz, 1H, H_8), 7.30 (s, 1H, H_6), 7.17 (d, $J_{11-10} = 8.25$, 1H, H_{11}), 6.98 (m, 2H, $H_{9,10}$), 6.83 (s, 1H, H_{13}), 6.06 (d, $J_{4-3} = 5.3$ Hz, 1H, H_4), 4.95 (t, $J_{3-4} \sim J_{3-2} = 6.3$ Hz, 1H, H_3), 3.30 (d, $J_{2-3} = 7.4$ Hz, 1H, H_2), 2.65 (s, 1H, H_{exo}); ^2H NMR (46 MHz, $C_6H_5CH_3$, 257K) δ 2.84 (s, 1D, D_{endo}); ^{13}C NMR (75 MHz, $C_6D_5CD_3$, 257 K) δ 225 (s(br), 3C, C≡O), 125−135 (8C, C_{6-13}), 108 (s, 1C, C_5), 107 (s, 1C, C_{14}), 97.0 (d, $J_{C4-H4} = 168$ Hz, 1C, C_4), 75.3 (d, $J_{C3-H3} = 179$ Hz, 1C, C_3), 50.7 (d, $J_{C2-H2} = 159$ Hz, 1C, C_2), 29.9 (dt, $J_{C1-Hexo} = 159$ Hz, 1C, C_1); mass spec (EI) *m/z*, 319 (14.9), 291 (66.0), 263 (50.0), 235 (48.5), 180 (100), 152 (9.0), 89 (6.5), 76 (7.5), 55 (16.2).

Results

Exploration of the reactivity of [Mn(η^4-$C_{14}H_{10}$)$(CO)_3$]$^-$ required access to the anion in synthetically convenient quantities. The existing preparation of the compound, however, gives access to the anion as a [K(Kryptofix 222)]$^+$ salt, which is too expensive for routine work.[4] To develop a more convenient preparation of the anion, we investigated metathesis of the initial anthracene substitution product K[Mn(η^4-$C_{14}H_{10}$)$(CO)_3$] with other cations.

Reaction of [Mn(η^6-C_6H_6)$(CO)_3$]PF_6 with K($C_{14}H_{10}$) and Isolation of [PPN][Mn(η^4-$C_{14}H_{10}$)$(CO)_3$]. The synthesis of [PPN][Mn(η^4-$C_{14}H_{10}$)$(CO)_3$] is similar to that of [K(Kryptofix 222)][Mn(η^4-$C_{14}H_{10}$)$(CO)_3$] ([K(Kryptofix 222)]**1**).[4] In both procedures, the reduction of [Mn(η^6-C_6H_6)$(CO)_3$]PF_6 with 2.2 equiv of K[$C_{14}H_{10}$] at −78 °C in THF resulted in the consumption of the cationic starting material (this was indicated by a change from a yellow slurry to an orange-brown solution and by the appearance of C≡O stretching bands in the infrared at 1940 (s), 1845 (s), and 1820 (s) cm^{-1}). The solution was allowed to warm to ambient temperature and was stirred overnight. Eighty-five percent of 1.0 equiv of [PPN]Cl was then added to the THF solution, and the mixture was stirred for 3 h. The solvent was removed to leave an orange powder, which was recrystallized from CH_2Cl_2 and Et_2O (1:3) to give large orange crystals of [PPN][Mn(η^4-$C_{14}H_{10}$)$(CO)_3$] ([PPN]**1**, 70%). The nature of the Mn(−I) anion in **1**$^-$ was established by its ^1H NMR spectrum, which is similar to that of [K(Kryptofix 222)]**1**.

The yield of [PPN]**1** is similar to that of [K(Kryptofix 222)]**1**, but metathesis must be carried out with less than a stoichiometric amount of [PPN]Cl because of the less than quantitative yield of [PPN]**1**. Use of a full equivalent of [PPN]Cl results in the presence of excess [PPN]Cl, and coprecipitation of [PPN]**1** and [PPN]Cl then inhibits the purification of [PPN]**1**.

The use of [K(18-crown-6)]$^+$ as a counterion for **1**$^-$ was also examined. The formation of [K(18-crown-6)]**1** occurred in a yield similar to that for the formation of [PPN]**1**, but crystals of [K(18-crown-6)]**1** grown from THF/Et_2O powdered under vacuum, presumably as a consequence of desolvation of Et_2O of crystallization.

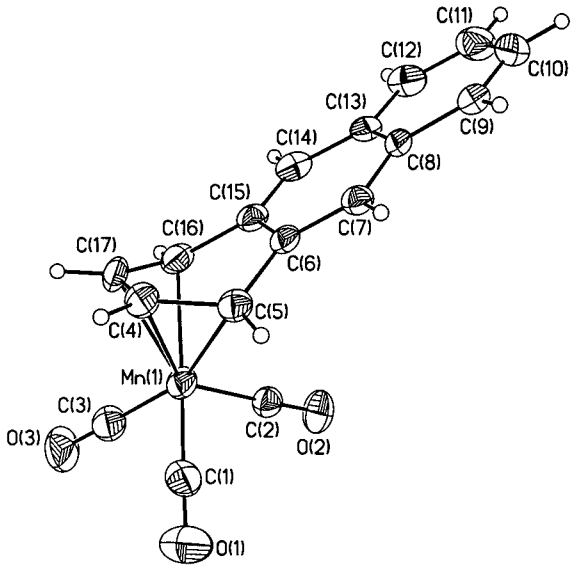

Figure 1. ORTEP drawing of the anion in [PPN][Mn(η^4-$C_{14}H_{10}$)$(CO)_3$] (35% probability ellipsoids).

This makes the isolation of [K(18-crown-6)]**1** difficult, and the $[PPN]^+$ salt of $\mathbf{1}^-$ is preferred.

The availability of $\mathbf{1}^-$ as the PPN^+ salt as well as the crystallographically characterized $[K(Kryptofix\ 222)]^+$ salt[4] offered an opportunity to test the assumption that the solid-state structures of η^4-arene complexes of $[Mn(CO)_3]^-$ are primarily controlled by electronic factors at the metal center and not by interactions with the counterions or packing forces.

The molecular structure of [PPN]**1** (Figure 1) was established by an X-ray diffraction analysis as described in the Experimental Section. The structure of the [Mn(η^4-$C_{14}H_{10}$)$(CO)_3]^-$ anion in [PPN]**1** is shown in Figure 1. Selected bond lengths and angles are listed in Table 3. The most notable feature of [PPN]**1** is the dihedral angle of 37.8(2)° between the coordinated diene and the exo naphthalene. This angle is much larger than the previously reported dihedral angle of 17.3° for the η^4-anthracene ligand in [Ni(η^4-$C_{14}H_{10}$)(η^2-depe)][10] but is similar to the dihedral angle of 31.5° for the η^4-anthracene ligand in [Ti(η^4-$C_{14}H_{10}$)(η^2-$C_{14}H_{10}$)(η^5-C_5Me_5)]$^-$ [11] and compares well with the η^4-naphthalene ligand in [PPN][Mn(η^4-$C_{10}H_8$)$(CO)_3$][2b] (dihedral angle of 37.1°) and the η^4-anthracene ligands in [K(Kryptofix 222)]**1** (34.9(2)°)[4b] and [Ti(η^6-$C_{14}H_{10}$)(η^4-$C_{14}H_{10}$)(η^2-dmpe)] (35.5°).[11]

Structural Comparison of [PPN][Mn(η^4-$C_{14}H_{10}$)$(CO)_3$] with [K(Kryptofix 222)][Mn(η^4-$C_{14}H_{10}$)$(CO)_3$]. Figures 2 and 3 depict least-squares fits of the anion in [K(Kryptofix 222)]**1**[4b] to that of the anion in [PPN]**1**. The solid line is the anion in [PPN]**1**, and the dashed line is the fitted structure. In Figure 2, the fit is made between all the non-hydrogen atoms of the anions in [K(Kryptofix 222)]**1** and [PPN]**1**. The average deviation between atomic positions within the structures is 0.214 Å. If the carbonyl ligands are not included in the fit, then the deviation between the two structures is only 0.102 Å (Figure 3). We conclude that the structures of the anions are almost identical and that the nature of the counterions has remarkably little effect on key structural parameters, such as the folding of the anthracene ligand.

Table 1. Crystal Data, Data Collection Parameters, and Agreement Factors for [PPN][Mn(η^4-$C_{14}H_{10}$)$(CO)_3$]

formula	$C_{53}H_{40}MnNO_3P_2$
fw	855.74
temp, K	223(2) K
wavelength, Å	0.71073
cryst syst	triclinic
space group	$P\bar{1}$
a, Å	12.384(7)
b, Å	14.147(9)
c, Å	15.085(9)
α, deg	117.07(5)
β, deg	109.05(5)
γ, deg	95.22(5)
V, *Z*, Å^3	2132(2), 2
ρ(calcd), Mg/m^3	1.333
μ, mm^{-1}	0.431
F(000)	888
crystal size, mm	0.21 × 0.27 × 0.32
θ range, deg	1.81−24.00
limiting indices	$-7 \le h \le 8$, $-16 \le k \le 16$, $-17 \le l \le 16$
no. of reflns collected	5334
no. of indep reflns	4984 (R_{int} = 0.0549)
abs corr	*ψ* scan
refinement method	full-matrix least squares on F^2
no. of data/restraints/params	4984/0/541
goodness of fit on F^2	1.034
final *R* indices [$I > 2\sigma(I)$]	R1 = 0.0425, wR2 = 0.0903
R indices (all data)	R1 = 0.0694, wR2 = 0.1042
largst diff peak and hole, e Å^{-3}	0.292 and −0.231

Table 2. Crystal Data, Data Collection Parameters, and Agreement Factors for [Mn(η^5-$C_{14}H_{11}$)$(CO)_3$]

formula	$C_{17}H_{11}MnO_3$
fw	318.2
temp, K	208(2) K
wavelength, Å	0.71073
cryst syst	monoclinic
space group	$P2_1/c$
a, Å	8.482(5)
b, Å	12.915(11)
c, Å	12.105(7)
α, deg	90
β, deg	90.30(4)
γ, deg	90
V, *Z*, Å^3	1326.1(15), 4
ρ(calcd), Mg/m^3	1.594
μ, mm^{-1}	1.001
F(000)	648
cryst size, mm	0.28 × 0.24 × 0.18
θ range, deg	2.31−24.05
limiting indices	$0 \le h \le 9$, $0 \le k \le 14$, $-13 \le l \le 13$
no. of reflns collected	2230
no. of indep reflns	2083 (R_{int} = 0.0344)
abs corr	*ψ* scan
refinement method	full-matrix least squares on F^2
no. of data/restraints/params	2083/0/235
goodness of fit on F^2	1.008
final *R* indices [$I > 2\sigma(I)$]	R1 = 0.0493, wR2 = 0.1073
R indices (all data)	R1 = 0.0845, wR2 = 0.1264
largst diff peak and hole, e Å^{-3}	0.562 and −0.354

Reactions of $[Mn(\eta^4\text{-}C_{14}H_{10})(CO)_3]^-$ with Electrophiles and Synthesis of [Mn(η^5-$C_{14}H_{11}$)$(CO)_3$]. Protonation of $\mathbf{1}^-$ was carried out at ambient temperatures by addition of 1.0 equiv of CF_3CO_2H to an orange-yellow slurry of [PPN][Mn(η^4-$C_{14}H_{10}$)$(CO)_3$] in *n*-pentane (Scheme 2). This resulted in a change to a wine-red

(10) Boese, R.; Stanger, A.; Stellberg, P.; Shazar, A. *Angew. Chem., Int. Ed. Engl.* **1993**, *32*, 1475.
(11) Seaburg, J. K.; Fischer, P. J.; Young, V. G.; Ellis, J. E. *Angew. Chem., Int. Ed.* **1998**, *37*, 155.

Table 3. Selected Bond Lengths (Å) and Angles (deg) within [PPN][Mn(η^4-$C_{14}H_{10}$)$(CO)_3$]

Mn−C(4)	2.073(4)	C(4)−C(5)	1.435(6)
Mn−C(5)	2.178(5)	C(16)−C(17)	1.418(6)
Mn−C(16)	2.183(4)	C(4)−C(17)	1.401(6)
Mn−C(17)	2.075(4)	C(5)−C(6)	1.453(6)
Mn−C(1)	1.780(5)	C(15)−C(16)	1.464(6)
Mn−C(2)	1.782(5)	C(6)−C(15)	1.449(6)
Mn−C(3)	1.767(7)	O(1)−C(1)	1.168(5)
O(3)−C(3)	1.173(5)	O(2)−C(2)	1.159(5)
C(1)−Mn−C(2)	98.2(2)	Mn−C(1)−O(1)	178.5(4)
C(2)−Mn−C(3)	98.2(2)	Mn−C(2)−O(2)	177.4(4)
C(3)−Mn−C(1)	91.4(2)	Mn−C(3)−O(3)	177.9(5)
C(4)−C(5)−C(6)	118.4(4)	C(17)−C(16)−C(15)	119.0(4)

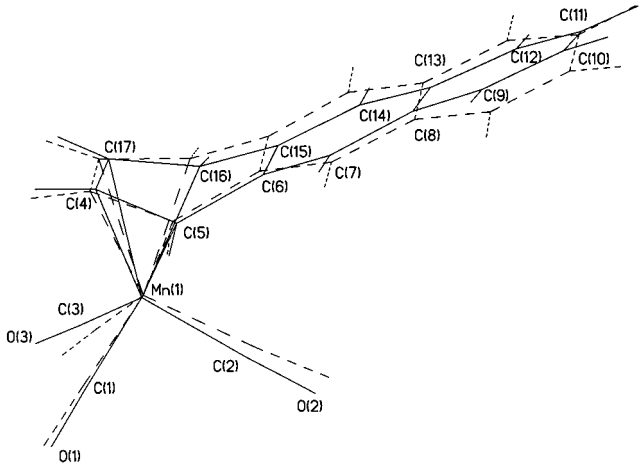

Figure 2. Least-squares fit for anions in [PPN][Mn(η^4-$C_{14}H_{10}$)$(CO)_3$] and [K(Kryptofix 222)][Mn(η^4-$C_{14}H_{10}$)$(CO)_3$], excluding the hydrogen atoms from the fitting program.

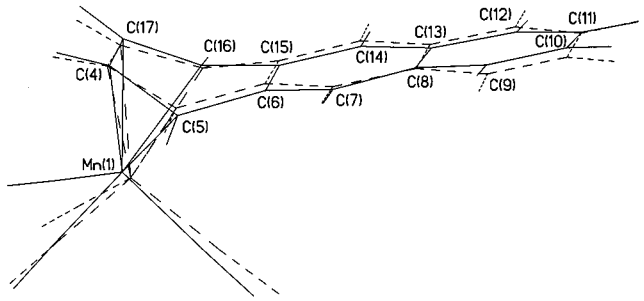

Figure 3. Least-squares fit for the anions in [PPN][Mn(η^4-$C_{14}H_{10}$)$(CO)_3$] and [K(Kryptofix 222)][Mn(η^4-$C_{14}H_{10}$)$(CO)_3$], excluding the hydrogen atoms and the CO ligands from the fitting program.

Scheme 2

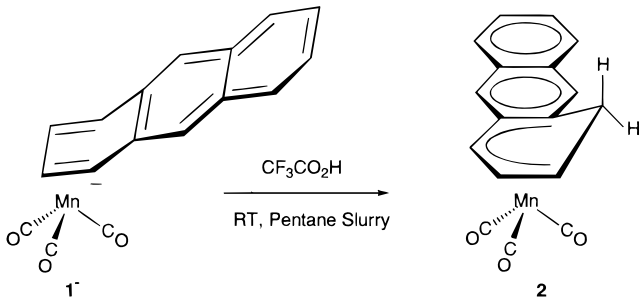

pentane solution containing a neutral manganese carbonyl complex (as indicated by the observation of C≡O stretching bands at 2020 (s), 1942 (s), and 1925 (s) cm^{-1}). The wine-red powder was recrystallized slowly from *n*-pentane at −15 °C to give small, red, air and water stable crystals of [Mn(η^5-$C_{14}H_{11}$)$(CO)_3$] (**2**, 38%). Fast recrystallization at −78 °C gave wine-red microcrystals of **2**.

The low yield in the protonation of [PPN]**1** partially reflects poor surface contact between [PPN]**1** and CF_3CO_2H in pentane, and we have examined the protonation reaction in THF, CH_3CN, and CH_2Cl_2, all of which are good solvents for [PPN]**1**. The protonation product of [PPN]**1** is unstable in THF and CH_3CN, and attempts to form **2** from solutions of [PPN][Mn(η^4-$C_{14}H_{10}$)$(CO)_3$] in THF or CH_3CN resulted in orange, pentane insoluble complexes with IR spectra that indicated the presence of unidentified neutral manganese carbonyl complexes. The product of protonation of [K(18-crown-6)]**1** was also unstable in THF and CH_3CN. The protonation of [PPN]-**1** to form **2** did occur in CH_2Cl_2 (as is indicated by the observation of C≡O stretching bands at 2010 (s), 1930 (s), and 1912 (s) cm^{-1} and a color change from orange to wine red), but removal of CH_2Cl_2 resulted in the decomposition of **2** into anthracene and unidentified manganese complexes.

We next examined the protonation of K[Mn(η^4-$C_{14}H_{10}$)-$(CO)_3$] in THF to determine if the presence of a coordinating counterion affected the course of the reaction. The addition of 1.0 equiv of CF_3CO_2H to a solution of K[Mn(η^4-$C_{14}H_{10}$)$(CO)_3$] formed in situ in THF did give **2** (65% spectroscopic yield). The solvent was immediately removed and the powder redissolved in pentane. Only microcrystalline **2** was obtained by this method, however, and the presence of excess anthracene frustrated attempts to isolate pure **2** by this procedure. It should be noted that complex **2** decomposes in THF after 30 min at ambient temperature into anthracene and unidentified manganese complexes.

Protonation could also be achieved by addition of 1.0 equiv of HPF_6 to a pentane slurry of [PPN]**1** to give **2**, but this offered no advantages over the CF_3CO_2H approach.

Attempts to add other electrophiles to $\mathbf{1}^-$ by reaction of [PPN]**1** or K**1** with $PhCH_2Cl$ and CH_3I were unsuccessful, and no reaction was observed. Preliminary reactions of [PPN]**1** with $CF_3SO_3CH_3$ indicate the formation of a neutral manganese carbonyl complex, but we have been unable to isolate a pure compound.

Structural Characterization of [Mn(η^5-$C_{14}H_{11}$)-$(CO)_3$]. The ^1H NMR spectrum of **2** has some unusual features (see below), and its molecular structure was therefore determined by an X-ray diffraction analysis (Figure 4). Selected bond lengths and angles for **2** are listed in Table 4.

Complex **2** has a nearly planar dienyl fragment, with the B and C aromatic rings attached at the first two atoms of the dienyl ligand and bent slightly below the plane (9.98(2)°). The cyclohexadienyl ring is folded about C2−C14, with a dihedral angle of 33.4(3)°. This dihedral angle is slightly smaller than the range of values determined for other cyclohexadienyl manganese complexes, ranging from 42° for [Mn(η^5-C_6H_7)$(CO)_3$],[12] 41° for [Mn{(η^5-$C_2H_5O_2C$)CH−C_6H_6}$(CO)_3$],[13] 40° for [Mn-{η^5-$C_6H_3(OCH_3)_3CH_2CN$}$(CO)_3$],[14] 39.6° for [Mn(η^5-PhC_6H_6)$(CO)_2NO$][BF_4],[15] 39.6° for [Mn{$(C_2H_5O)_2P(O)$-

(12) Churchill, M. R.; Scholer, F. R. *Inorg. Chem.* **1969**, *8*, 1950.
(13) Mawby, A. *J. Organomet. Chem.* **1973**, *55*, C39

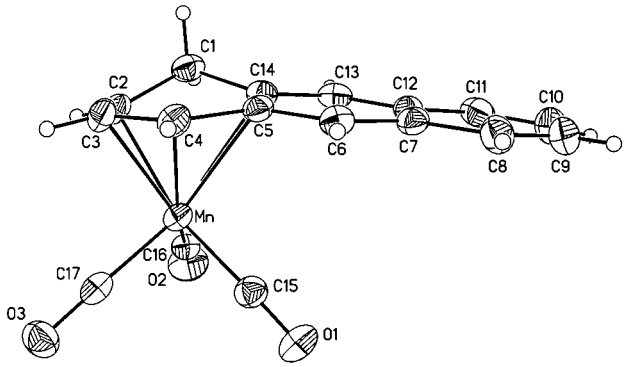

Figure 4. ORTEP drawing of [Mn(η^5-$C_{14}H_{11}$)$(CO)_3$] (35% probability ellipsoids).

Table 4. Selected Bond Lengths (Å) and Angles (deg) within [Mn(η^5-$C_{14}H_{11}$)$(CO)_3$]

C(1)−C(14)	1.503(7)	Mn−C(2)	2.155(5)
C(1)−C(2)	1.487(7)	Mn−C(3)	2.095(5)
C(2)−C(3)	1.378(8)	Mn−C(4)	2.095(5)
C(3)−C(4)	1.392(7)	Mn−C(5)	2.296(5)
C(4)−C(5)	1.433(6)	Mn−C(14)	2.485(5)
C(5)−C(14)	1.412(7)	Mn−C(15)	1.790(5)
C(5)−C(6)	1.385(6)	Mn−C(16)	1.779(6)
C(14)−C(13)	1.380(7)	Mn−C(17)	1.728(6)
O(1)−C(15)	1.133(6)	O(3)−C(17)	1.167(6)
O(2)−C(16)	1.145(6)	Mn−cy[a]	1.757(5)
Mn−C(15)−O(1)	178.3(5)	C(17)−Mn−C(16)	93.2(2)
Mn−C(16)−O(2)	178.1(5)	C(17)−Mn−C(15)	88.1(2)
Mn−C(17)−O(3)	178.2(4)	C(16)−Mn−C(15)	98.9(2)
Mn−cy−C(15)[a]	120.8(2)	Mn−cy−C(17)[a]	127.7(2)
Mn−cy−C(16)[a]	120.2(2)	C(1)−C(2)−C(14)	108.0(4)

[a] cy = centroid of the dienyl portion of the anthracenyl ligand.

(η^5-C_6H_6)}$(CO)_3$],[16] 38° for [Mn{η^5-$C_6H_6CH_2C(NCH_3Ph)$═W$(CO)_5$}$(CO)_3$],[17] 36.5° for [Mn(η^5-PhC_6H_6)$(CO)_3$],[15] 36.8° for [Mn{η^5-C_6H_6-*exo*-(Me_3SiCN_2)}$(CO)_3$],[18] 36° for [{Mn$(CO)_3$}$_2$-{μ-(η^5-C_6H_6CHCN-η^5-C_6H_6)}],[14] to 35° for [Mn{η^5-$C_6H_6CCH_3ClCO_2CH_3$}$(CO)_3$].[19] The small dihedral angle in complex **2** most likely reflects the influence of the fused π system attached at C14 and C5, and a similar decrease in dihedral angle to 29.6° is observed for [Mn{η^5-C_8H_6NH-*exo*-(CMe_2CN)}$(CO)_3$],[20] which also contains a fused aromatic ligand. The torsion angles between the endo and exo C−H bonds on C1 and the vicinal C−H bond on the dienyl ligand in **2** are 85.1° for H2−C2−C1−H_{exo} and 30.9° for H2−C2−C1−H_{endo}; the latter is unusually large for a cyclohexadienyl complex of "Mn$(CO)_3$", as required by the small folding of the cyclohexadienyl ring.

An additional consequence of the presence of the fused π system is the lengthening of the manganese to carbon bonds at the fused carbons. For example, in complex **2** the Mn−C(2,3,4) is ∼2.115(5) Å (∼2.137 Å for [Mn{η^5-C_8H_6NH-*exo*-(CMe_2CN)}$(CO)_3$][20]), Mn−C5 is 2.296(5) Å, and Mn−C14 is 2.485(5) Å (2.266 and 2.434 Å for [Mn-{η^5-C_8H_6NH-*exo*-(CMe_2CN)}$(CO)_3$][20]).

Table 5. Comparison of Aromatic C−C Bond Lengths (Å) in [Mn(η^5-$C_{14}H_{11}$)$(CO)_3$] to Similar Organometallic Complexes and Anthracene

[Mn(η^5-$C_{14}H_{11}$)$(CO)_3$]	1.389 ± 0.028
[Mn(η^5-C_6H_7)$(CO)_3$][12]	1.401 ± 0.014
[Mn{η^5-C_6H_6-*exo*-(Me_3SiCN_2)}$(CO)_3$][18]	1.399 ± 0.016
[Mn{η^5-C_8H_6NH-*exo*-(CMe_2CN)}$(CO)_3$][20]	1.409 ± 0.032
$C_{14}H_{10}$[32]	1.409 ± 0.029

The average C−C bond length for the aromatic ring system in **2** is compared with similar figures for related complexes in Table 5. The geometry of the "Mn$(CO)_3$" fragment in **2** is unexceptional.

Variable-Temperature ^{1}H NMR Spectra of [Mn(η^5-$C_{14}H_{11}$)(CO_3)]. The ^{1}H NMR spectra of complex **2** at various temperatures are shown in Figure 5. The temperature-dependent changes in the ^{1}H NMR spectra of **2** are fully reversed when the sample is warmed. It was not feasible to examine spectra at temperatures much above ambient, because the compound is thermally unstable. At room temperature (297 K), lines in the spectrum are broad and provide minimal structural information.

The peaks in the 297 K spectrum at 6.10, 4.99, and 3.35 δ each integrate as one proton, while the group of peaks centered at 2.76 δ integrates as two protons. The remaining six protons resonate in the aromatic region of the spectrum. As the sample is cooled to 287 K, the group of peaks centered at 2.76 δ begins to sharpen and a shoulder forms at 6.89 δ. At 277 K, two distinct resonances can be observed at 2.68 and 2.83 δ, the peaks between 6.50 and 3.00 δ all begin to show H−H coupling, and the peaks in the aromatic region of the spectrum begin to sharpen. Finally, at 257 K definite splitting patterns that correspond to the assignments listed in Table 6 are observed for each proton resonance of [Mn(η^5-$C_{14}H_{11}$)$(CO)_3$]. The endo and exo protons were assigned according to the Karplus relation:[21] the torsion angle between the H_{exo} and H_{ortho} protons is 85.1°, between the H_{endo} and H_{ortho} protons the torsion angle is 30.9°, and the angle that is closer to 90° will correspond to a smaller coupling constant. In complex **2**, the vicinal coupling constant observed for each doublet in the peak centered at 2.84 δ is 4.9 Hz, but vicinal coupling is not observable for the doublet at 2.66 δ. The resonance at 2.66 δ is therefore assigned to the exo proton and the resonance at 2.84 δ is assigned to the endo proton of [Mn(η^5-$C_{14}H_{11}$)$(CO)_3$], with a vicinal coupling constant to the ortho hydrogen smaller than the typical 6 Hz value[1a] as a consequence of the small dihedral angle subtended by the methylene group.

The temperature-dependent broadening of the ^{1}H NMR spectrum was unexpected, in part because the related cyclohexadienyl complexes [Mn(η^5-C_6H_7)$(CO)_3$][22] and [Mn(η^5-$C_{10}H_9$)$(CO)_3$][2b] do not exhibit unusual ^{1}H NMR spectra at ambient temperatures. The origin of the broadening was difficult to determine at first because so many resonances were affected in such a

(14) Rose, E.; Le Corre-Susanne, C.; Rose-Munch, F.; Renard, C.; Gagliardini, V.; Teldji, F.; Vaisserman, J. *Eur. J. Inorg. Chem.* **1999**, 421.
(15) Ittel, S. D.; Whitney, J. F.; Chung, Y. K.; Williard, P. G.; Sweigart, D. A. *Organometallics* **1988**, *7*, 1323.
(16) Lee, T.; Yu, H. B.; Chung, Y. K.; Hallows, W. A.; Sweigart, D. A. *Inorg. Chim. Acta* **1994**, *224*, 147.
(17) Rose-Munch, F.; Le Corre-Susanne, C.; Balssa, F.; Rose, E.; Vaisserman, J.; Licandro, E.; Papagni, A.; Maiorana, S.; Meng, W.; Stephenson, G. R. *J. Organomet. Chem.* **1997**, *545*−*546*, 9.
(18) Reau, R.; Reed, R. W.; Dahan, F.; Bertrand, G. *Organometallics* **1993**, *12*, 1501.
(19) Balssa, F.; Gagliardini, V.; Le Corre-Susanne, C.; Rose-Munch, F.; Rose, E.; Vaisserman, J. *Bull. Soc. Chim. Fr.* **1997**, *134*, 537.
(20) Ryan, W. J.; Peterson, P. E.; Cao, Y.; Williard, P. G.; Sweigart, D. A.; Baer, C. D.; Thompson, C. F.; Chung, Y. K.; Chung, T. M. *Inorg. Chim. Acta* **1993**, *211*, 1.
(21) Karplus, M. *J. Chem. Phys.* **1959**, *30*, 11.
(22) Lamanna, W.; Brookhart, M. *J. Am. Chem. Soc.* **1980**, *102*, 3490.

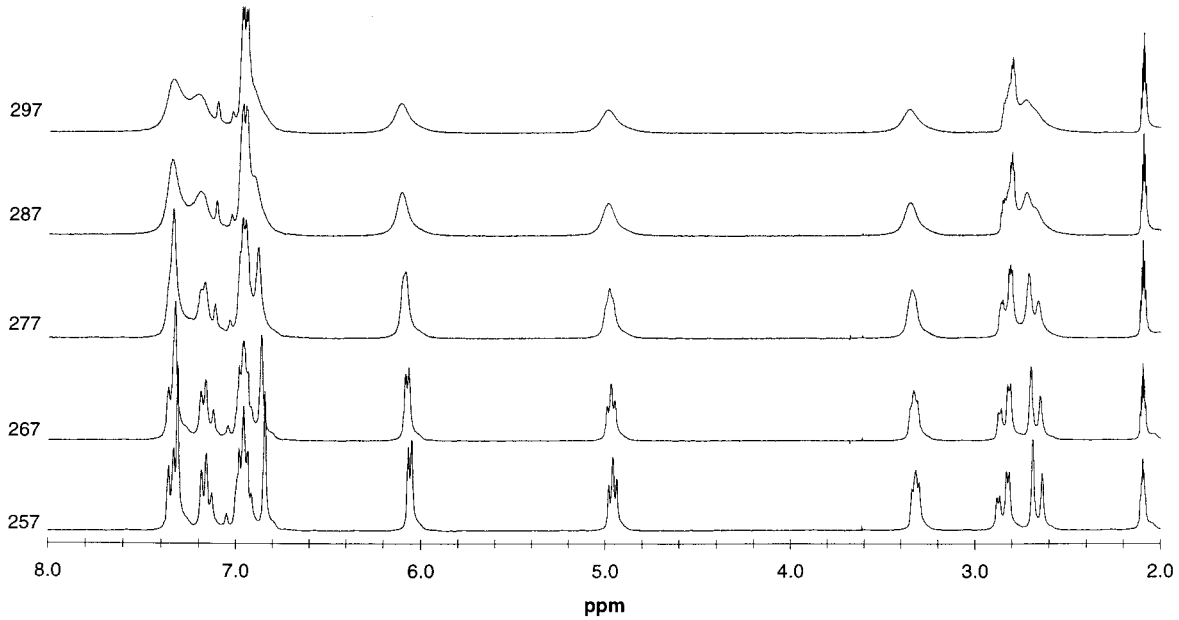

Figure 5. Variable-temperature ^{1}H NMR spectra of [Mn(η^5-$C_{14}H_{11}$)$(CO)_3$] (300 MHz, $C_6D_5CD_3$).

Table 6. ^{1}H NMR Spectrum Assignments (ppm) for [Mn(η^5-$C_{14}H_{11}$)$(CO)_3$]

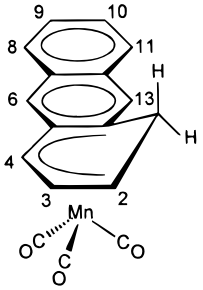

H_{exo}	2.66	(d, $J_{exo-endo}$ = 15.4 Hz)
H_{endo}	2.84	(dd, $J_{endo-exo}$ = 15.4 Hz, J_{endo-2} = 4.9 Hz)
H_2	3.32	(t, $J_{2-endo} \sim J_{2-3}$ = 5.9 Hz)
H_3	4.96	(t, $J_{3-2} \sim J_{3-4}$ = 6.4 Hz, 1H)
H_4	6.06	(d, J_{4-3} = 5.6 Hz, 1H)
H_{13}	6.84	(s, 1H)
$H_{9,10}$	6.96	(dt, 2H)
H_{11}	7.17	(d, J_{11-10} = 8.23 Hz, 1H)
H_6	7.31	(s. 1H)
H_8	7.35	(d, J_{8-9} = 8.23 Hz, 1H)

uniform manner. To explore the origin of the line broadening, magnetization transfer experiments were conducted.

Magnetization Transfer and NOE Difference Spectra of [Mn(η^5-$C_{10}H_9$)$(CO)_3$].[23] NOE (nuclear Overhauser enhancement) difference spectra of **2** were recorded at 257 K. The pulse sequence for NOE experiments involves irradiating one resonance of the spectrum and then applying a $\pi/2$ observation pulse to record the FID. If exchange occurs with the irradiated proton, magnetization will be transferred from the irradiated proton to one or more other protons in the system and will be observed through a reduction in signal strength wherever exchange occurs.

Figure 6 shows the difference spectra obtained by subtracting NMR spectra recorded with and without narrow band irradiation of specified nuclei (H^*). The convention for subtraction was [(H^* at *x* ppm spectrum) − (H^* at 0.00 ppm spectrum)].

When the peak at 6.06 δ (or 2.66 δ) is irradiated, the difference spectrum contains two negative peaks, one very large at 6.06 δ (or 2.66 δ) and a small negative peak at 2.66 δ (or 6.06 δ), which implies that magnetization is transferred between the exo proton and the proton para to the methylene group in the cyclohexadienyl ligand. Irradiation applied at 2.84 δ causes only the peak at 2.84 δ to invert after subtraction of the spectra, establishing that there is no exchange between the endo proton and other ring protons. Irradiation at 4.96 δ (or 3.32 δ) gives an additional negative peak at 3.32 δ (or 4.96 δ), and irradiation at 7.17 δ (or 7.31 δ) yields a negative peak at 7.31 δ (or 7.17 δ).

These exchange spectra suggest that the exo proton is exchanging with the proton in the para orientation. This would account for all of the observed magnetization transfers, and a low barrier to such an exchange would be consistent with a metal-mediated intermediate (Scheme 3) in which the proton of the trifluoroacetic acid adds first to the metal to give the metal hydride intermediate **A** and then moves up to the ring into one of two symmetrically equivalent positions. What the NMR data suggest is that this migration is reversible. The magnetization transfer data incidentally confirm the previous assignment of the endo ^{1}H resonance based on the Karplus relationship, and the exchange sequence agrees with all of the assignments made for ^{1}H NMR spectra of complex **2**.

Quantitative Analysis of Fluxional Process in [Mn(η^5-$C_{14}H_{11}$)$(CO)_3$]. Simulations of the dynamic ^{1}H NMR spectra,[24] in terms of the proposed mechanism, were carried out in order to determine the rate of exchange between the two proton environments and provide insight into the underlying dynamic processes.

(23) (a) Sanders, J. K.; Hunter, B. K. In *Modern NMR Spectroscopy: A Guide for Chemists*; Oxford University Press: New York, 1990, Chapters 1−3, 6, and 17. (b) Noggle, J. H.; Schirmer, R. E. In *The Nuclear Overhauser Effect*; Academic Press: New York, 1971, Chapters 1 and 7. (c) Forsen, S.; Hoffman, R. A. *J. Chem. Phys.* **1963**, *39*, 2892.

(24) The DNMR3 program (http://www.arl.hpc.mil/PET/cta/ccm/software/qcpe/QCPE2/index.html) was used to simulate the ^{1}H NMR spectra: (a) Kleier, D. A.; Binsch, G. *QCPE* **1970**, *11*, 165. (b) Binsch, G.; Kessler, H. *Angew. Chem., Int. Ed. Engl.* **1980**, *19*, 411.

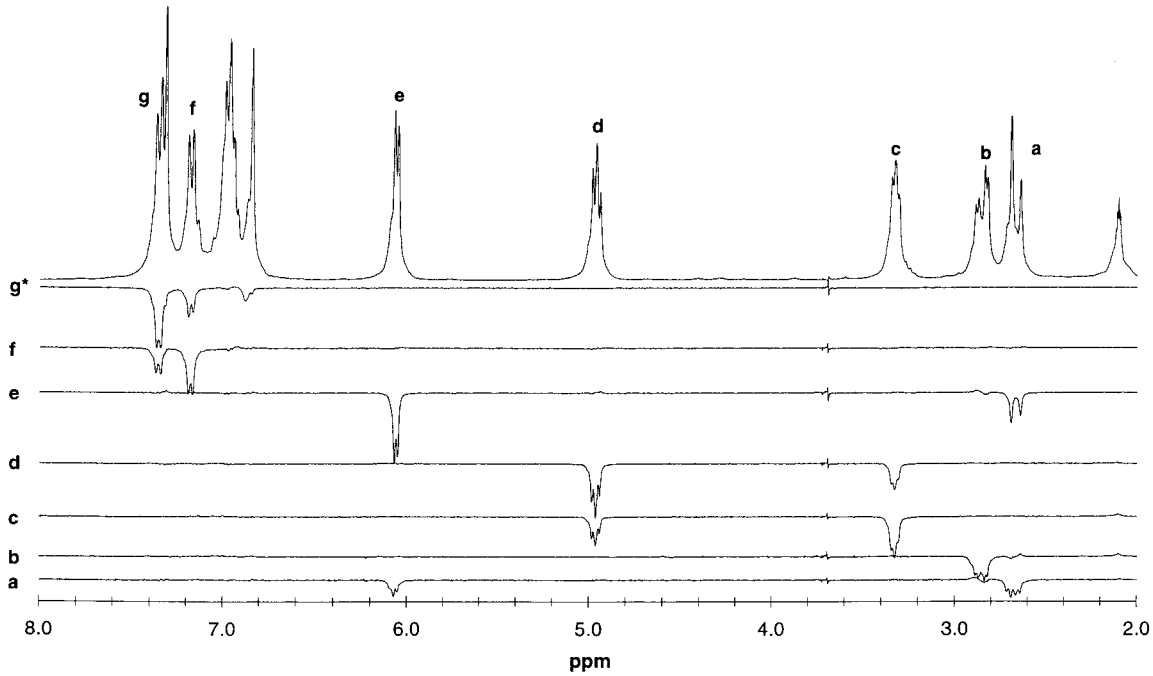

Figure 6. NOE difference spectra of [Mn(η^5-$C_{14}H_{11}$)$(CO)_3$] at 257 K (300 MHz, $C_6D_5CD_3$). The difference spectra are labeled with letters that correspond to the peak being irradiated. In spectrum g*, the peak at 6.84 is inverted because of the breadth of the irradiation at 7.35 δ.

Scheme 3

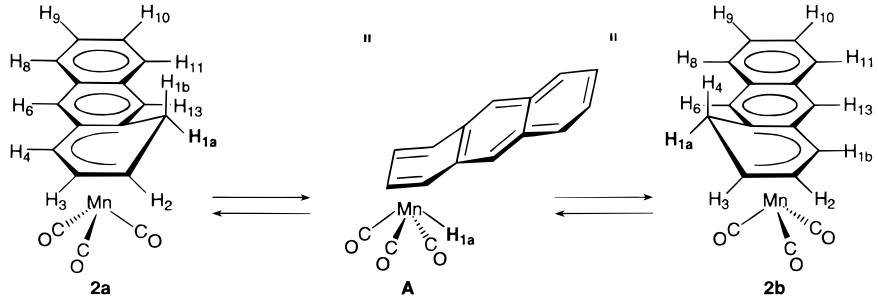

Spectra were acquired between 257 and 297 K at 5 K intervals, and line shapes for the region between 6.5 δ and 2.5 δ were simulated for each spectrum. Attempts to carry out a least-squares fit of simulated to experimental line widths for all peaks in the spectrum did not converge, but convergent fits were obtained when the resonances were treated in two groups, one comprised of the "outside" (exo, endo, and para) proton resonances, and the other comprised of the "inside" (ortho and meta) proton resonances. Figures 7 and 8 show stacked plots of the simulated and calculated spectra for the two types of fits. Because each proton in **2** is uniformly affected by the hydride migration reaction (Scheme 3), the line shape data obtained for each group can be considered collectively. The simulated exchange rates at each temperature, the averaged ("mean") exchange rates at each temperature, and the corresponding activation energies for the 1,4-hydride migration between the two equivalent sites on the anthracene ligand are summarized in Table 7. The Eyring plot[25] of the data shown in Figure 9 gives rise to an enthalpy of activation for the migration of 12.3 ± 0.2 kcal/mol and a small negative entropy of activation of −7.7 ± 0.8 eu.

Table 7. Rates of Exchange for 1,4-Hydride Shift in [Mn(η^5-$C_{14}H_{11}$)$(CO)_3$] Calculated from Line Shape Analysis

T (K)	k (s^{-1}) "outside"	k (s^{-1}) "inside"	k (s^{-1}) "mean"	ΔG (kcal/mol)
257	4.0	4.0	4.0	14.3
262	6.5	5.5	6.0	14.3
267	10.5	8.50	9.50	14.4
272	13.5	20.5	17.0	14.3
277	20.0	28.0	24.0	14.4
282	29.0	40.0	34.5	14.5
287	50.0	50.0	50.0	14.5
292	82.5	80.0	81.25	14.5
297	108.0	125.0	116.25	14.6

Deuterium Labeling and Kinetic Isotope Effect on Fluxionality within [Mn(η^5-$C_{14}H_{10}D$)$(CO)_3$]. The reaction of [PPN][Mn(η^4-$C_{14}H_{10}$)$(CO)_3$] with 1.0 equiv of

(25) (a) Sandstrom, J. In *Dynamic NMR Spectroscopy*; Academic Press: London, 1982; Chapter 7. (b) Glasstone, S.; Laidler, K.; Eyring, H. In *The Theory of Rate Processes*; McGraw-Hill: New York, 1941; p 195. (c) Eyring, H. *Chem. Rev.* **1935**, *17*, 65.

(26) Failure to always incorporate a full equivalent of deuterium into **3** (^{1}H NMR confirms 90% incorporation) prevented us from performing line shape analysis on **3**. Early ^{1}H NMR samples of **3** show full incorporation of deuterium into the endo position and allowed us to estimate rates based upon the experimental line widths. In no case have we seen incorporation of deuterium into the exo position. Similar observations have been reported for [Mn(η^5-$C_6H_7(CO)_3$] and [Mn(η^5-$C_{10}H_9(CO)_3$]; see ref 2b.

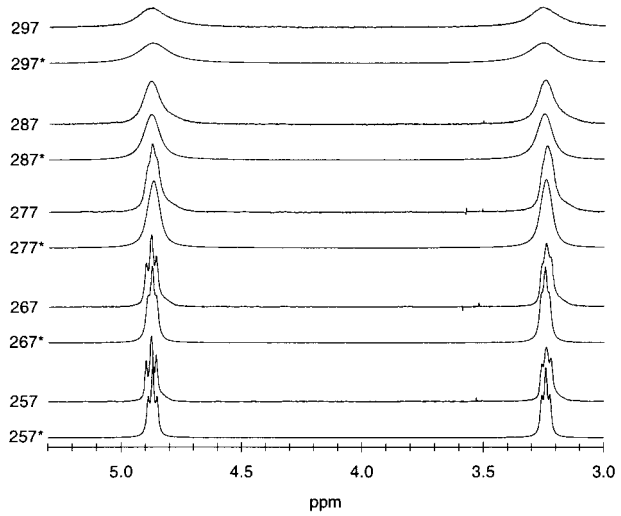

Figure 7. Variable-temperature ^{1}H NMR spectra of [Mn(η^5-$C_{14}H_{11}$)$(CO)_3$] (300 MHz, $C_6D_5CD_3$) with calculated line shapes of the ortho and meta (inside) proton resonances, observed vs calculated (*).

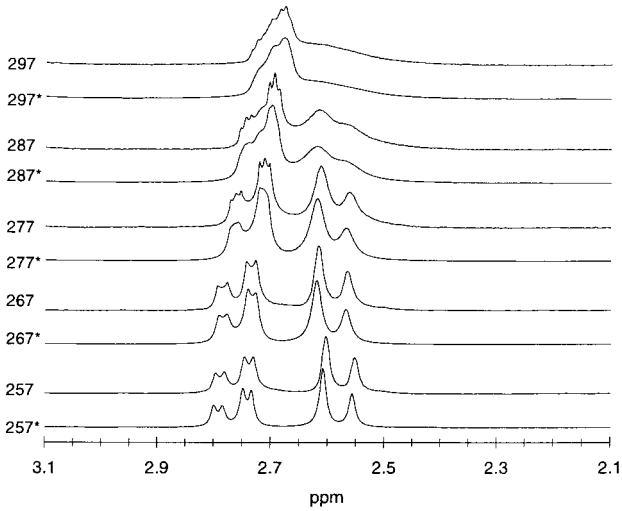

Figure 8. Variable-temperature ^{1}H NMR spectra of [Mn(η^5-$C_{14}H_{11}$)$(CO)_3$] with calculated line shapes of the endo and exo (outside) proton resonances, observed vs calculated (*).

CF_3CO_2D proceeds quantitatively to give [Mn(η^5-$C_{14}H_{10}D$)$(CO)_3$] (**3,** 42%) under the same reaction conditions reported for the formation of **2** (see above). Complex **3** was recrystallized slowly from *n*-pentane at −15 °C to give small red air stable crystals. Deuteration occurs primarily in the endo position of the η^5-bound ring.[26]

The ^{1}H NMR spectrum of **3** exhibits temperature-dependent broadening similar to that observed in the spectra of **2**, but when spectra of **3** are compared with spectra of **2** as the temperature is decreased, the ^{1}H NMR resonances of **3** sharpen more quickly than the resonances of **2**. It is clear that complex **3** participates in an exchange sequence similar to that established for complex **2** (Scheme 3), but at a slower rate. We could not obtain convergent simulations of spectra of complex **3**,[26] but a kinetic isotope effect (k_H/k_D) of 1.88 could be estimated on the basis of the line widths of the experimental spectra.[27] The observation that the exchange sequence is slower for the deuterated complex than for the protonated complex implies that there is considerable bond breaking involving the C−H(D) bond in the transition state for the exchange reaction and not much compensating bond making, and this inference is consistent with the transition state shown in the proposed mechanism (see below, Scheme 5).

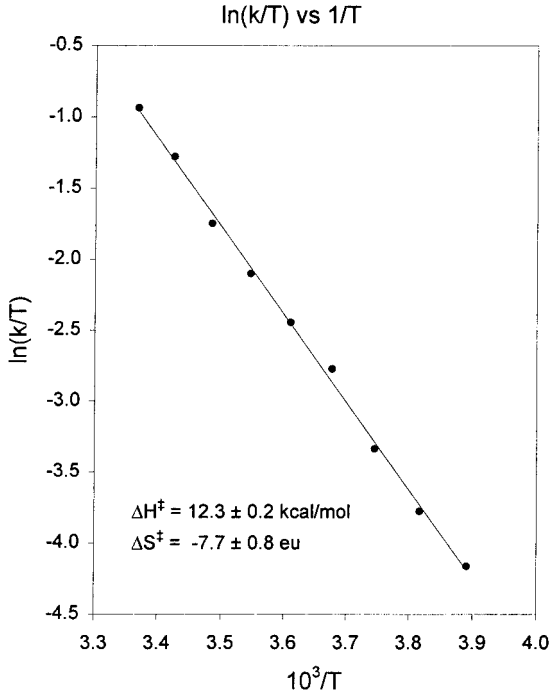

Figure 9. Eyring plot for the 1,4-hydride shift in [Mn(η^5-$C_{14}H_{11}$)$(CO)_3$] in $C_6D_5CD_3$. The errors reported in the activation parameters are based on the method of least squares and are calculated from the standard deviations in the slope and *y*-intercept.

Discussion

We have shown that protonation of the terminal (η^4-anthracene) manganese tricarbonyl anion [Mn(η^4-$C_{14}H_{10}$)$(CO)_3]^-$ (**1**$^-$) occurs at the end ring to give the (η^5-anthracenyl) manganese tricarbonyl complex [Mn(η^5-$C_{14}H_{11}$)$(CO)_3$] (**2**), and this metal-mediated addition of the corresponding anthracene therefore has a regioselectivity complementary to that observed in conventional organic reductions of anthracene. Single-crystal X-ray diffraction analysis confirms the addition of the proton to the hydrocarbon ring, and labeling studies establish that protonation is regiospecific and occurs at the endo site.

Dynamic ^{1}H NMR studies and magnetization transfer experiments establish that **2** is fluxional and that an overall 1,4-hydride shift reaction equilibrates the two sides of the anthracenyl ligand on the NMR time scale. The data that we have been able to acquire delineate the process to the level of detail shown in Scheme 3, but this does not fully describe the mechanism of the reaction: the classic study by Lamanna and Brookhart[22] on the thermal isomerization of 6-*exo*-^{1}H-[Mn(η^5-C_6-

(27) (a) Thompson, R. L.; Lee, S.; Geib, S. J.; Cooper, N. J. *Inorg. Chem.* **1993**, *32*, 6067. (b) Binsch, G. *Top. Stereochem.* **1968**, *3*, 97. (c) Binsch, G. In *Dynamic Nuclear Magnetic Resonance Spectroscopy*; Jackman, L. M., Cotton, F. A., Eds.; Academic Press: New York, 1975; Chapter 3.

Scheme 4

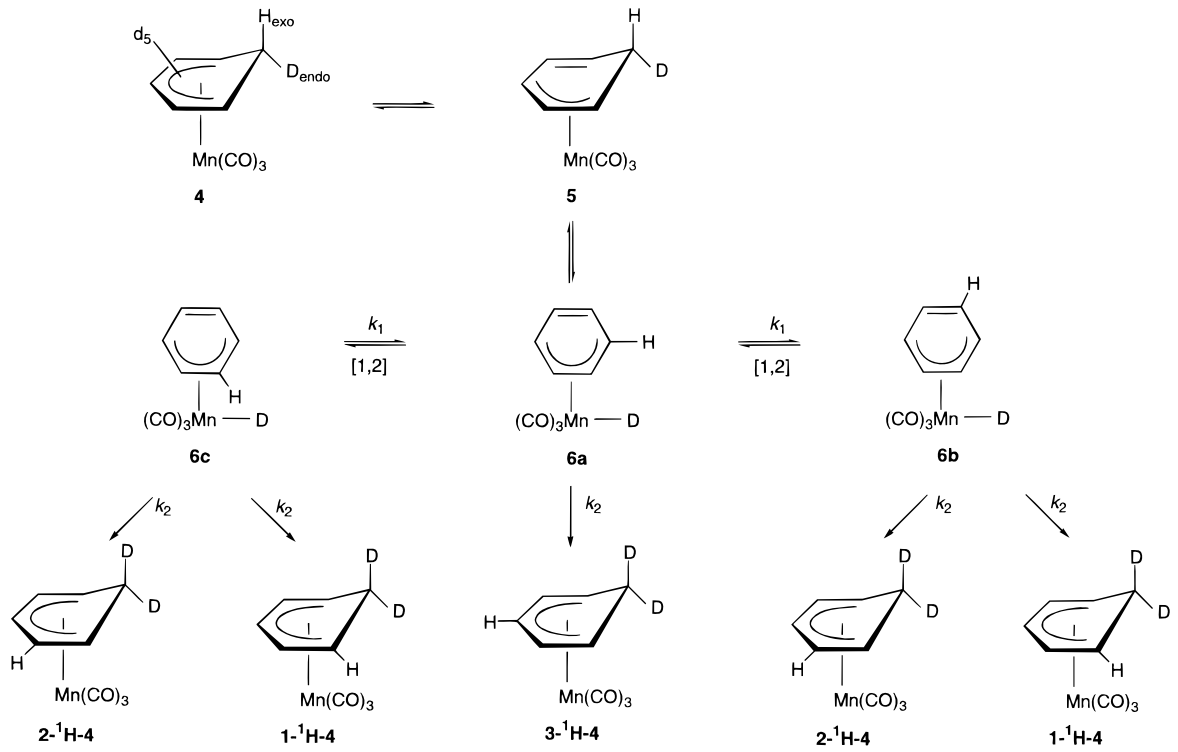

Scheme 5

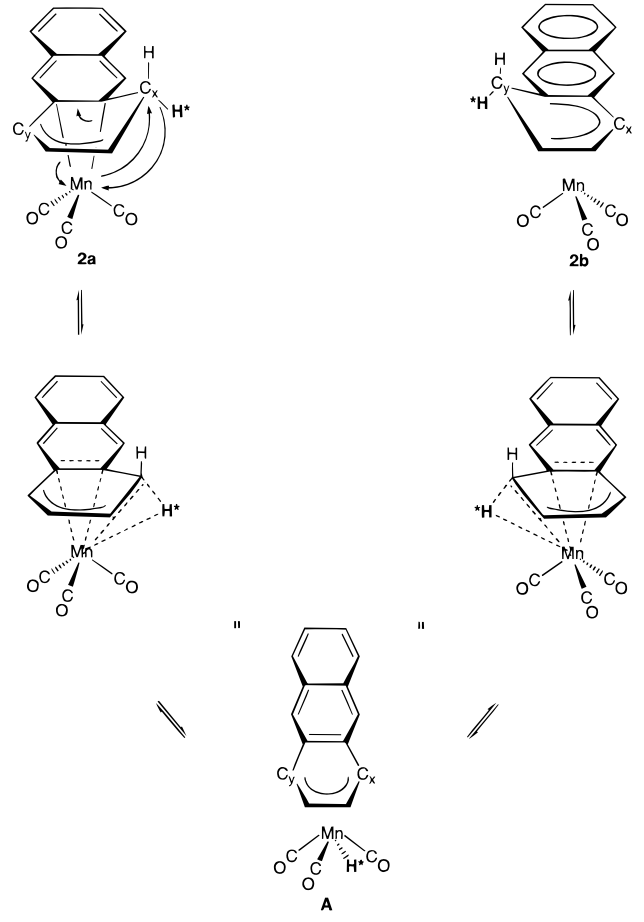

$HD_5)(CO)_3$] both facilitates and requires a more detailed discussion of the reaction pathway.

The Lamanna and Brookhart study proposes the mechanism shown in Scheme 4[22] for hydride (deuteride) migration within 6-*exo*-^{1}H-[Mn(η^5-C_6HD_5)$(CO)_3$] (**4**). This adds two additional steps to the mechanism in Scheme 3: an η^5 to η^3 hapticity shift in the dienyl ligand that precedes the carbon to manganese hydride shift, and 1,2 shifts of the metal around the polyene ligand in the intermediate η^4-diene complex **6a**. These steps are invoked to explain why the intramolecular carbon to manganese hydride shift can lead to isomerization, since the observed isomerization requires that the hydride return to a different carbon atom when it moves back to the metal center. This proposal is supported by its ability to provide a comprehensive framework for the interpretation not only of isomerization within **4** but also of hydride migration within phenyl- and methyl-substituted analogues of **4** as first established and analyzed by Pauson.[28]

Fluxionality within **2** poses problems similar to those addressed by Lamanna and Brookhart, since there must be a process by which the hydride in intermediate **A** returns from the metal to a different carbon atom in the hydrocarbon ligand without violating microscopic reversibility. We propose, however, an interpretation (Scheme 5) that differs in two important respects from Scheme 4:

(1) The η^5 to η^3 shift in Scheme 4 is less attractive today in light of our understanding of how agostic and other σ donation interactions maintain 18-electron configurations in low-valent environments;[29] we therefore propose a migration step in which increased interaction of the hydride with the metal center is synchro-

(28) (a) Munro, G. A. M.; Pauson, P. L. *J. Chem. Soc., Chem. Commun.* **1976**, 134. (b) Pauson, P. L.; Segal, J. A. *J. Chem. Soc., Dalton Trans.* **1975**, 1677. (c) Pauson, P. L.; Segal, J. A. *J. Chem. Soc., Dalton Trans.* **1975**, 1683.

(29) (a) Crabtree, R. H. *Angew. Chem., Int. Ed. Engl.* **1993**, *32*, 789. (b) Brookhart, M.; Green, M. L. H.; Wong, L.-L. *Prog. Inorg. Chem.* **1988**, *36*, 1. (c) Brookhart, M.; Green, M. L. H. *J. Organomet. Chem.* **1983**, *250*, 395.

nous with deligation of the carbons carrying the aromatic substituent.

(2) We do not believe it is necessary to invoke a 1,2-manganese shift step. Return of the hydride to carbon "*y*" instead of degenerate return to carbon "*x*" can be explained in terms of fluxionality within the four-legged piano stool and averaging of the carbonyl ligands and a hydride in **A**; with the sterically undemanding hydride ligand, such an isomerization could have a low energy barrier. Alternatively, the hydride in the intermediate **A** could be positioned symmetrically between carbon "*x*" and carbon "*y*" as shown in Scheme 5, and return to carbon "*x*" or carbon "*y*" would then occur with equal probability. Such a symmetric positioning of the hydride in the intermediate could contribute to the low height of the energy barrier observed for isomerization of **2**.

The data to hand (or readily accessible) do not provide a definitive basis for choosing between Scheme 4 and Scheme 5, and a mechanism analogous to that in Scheme 4 is a feasible interpretation on the assumption that $k_1 \gg k_2$ and that there is a thermodynamic preference for the anthracenyl isomer in which the aromatic substitution is in the 2,3 (or the degenerate 5,6) position.

This interpretation is, however, difficult to reconcile with our understanding of the free energy reaction coordinates in these systems, and the small 14.5 kcal/mol isomerization barrier in **2** argues that Scheme 5 offers a more satisfying interpretative framework. It is reasonable, for example, that the aromatic substituent on the dienyl ligand in **2** could stabilize the transition state for the synchronous hydride shift shown in Scheme 5 and that it could lower the free energy difference between **2** and **A** below the 14−19 kcal/mol energy difference suggested for **4** and **6a** by Lamanna and Brookhart;[22] additionally the 33.3° dihedral angle for the folding of the methylene group in the dienyl fragment in $[Mn(\eta^5\text{-}C_{14}H_{11})(CO)_3]$ is smaller than the value of 42° for $[Mn(\eta^5\text{-}C_6H_7)(CO)_3]$[12] and would place the endo hydrogen closer to the metal in the anthracenyl complex and hence facilitate the migration.

It is much more difficult to interpret the marked difference between the barriers to isomerization observed for **4** and **2** within the context of Scheme 4. The kinetic isotope effect that we have observed in the isomerization of **2** establishes that the rate-determining step must involve C−H bond cleavage, and the 1,2-manganese shift would then have to have a lower activation barrier than this step. The 1,2-manganese shift barrier is, however, a combination of two free energy differences: the base ΔG between **2** and intermediate **A**, argued by Lamanna and Brookhart to be about 14−19 kcal/mol in the parent cyclohexadienyl system,[22] and the activation barrier to the 1,2-manganese polyene shift itself, established by Whitesides[30] and Maitlis,[31] as reviewed by Lamanna and Brookhart,[22] to be ca. 14 kcal/mol. It is difficult to see how the aromatic substituent in **2** could so dramatically lower both of these components of the free energy difference that their sum could become significantly less than the observed 14.5 kcal/mol barrier to the rate-determining C−H bond cleavage step.

We conclude that we prefer the analysis of the fluxional process proposed in Scheme 5; this offers a pathway close to the least motion pathway for the process since it makes movement of the hydrogen atom, by far the lightest atom in the system, the central feature of each step in the isomerization. The discovery that the barrier to isomerization in **2** is dramatically less than the barrier to isomerization established for **4** may also require minor modification of the interpretation previously proposed for the isomerization of **4**.

Acknowledgment. This work was financially supported by the NSF through grant numbers CHE 9632202 (N.J.C.) and CHE 9615116 (G.F.).

Supporting Information Available: Complete X-ray crystallographic data for [PPN]**1** and **2** and complete dynamic ^{1}H NMR spectra for the line shape analysis of complex **2** are available at http://www.pubs.acs.org.

OM990735G

(30) Whitesides, T. H.; Budnik, R. A. *Inorg. Chem.* **1976**, *15*, 874.
(31) Kang, J. W.; Childs, R. F.; Maitlis, P. M. *J. Am. Chem. Soc.* **1970**, *92*, 720.
(32) (a) Mathieson, A.; Robertson, J. M.; Sinclair, V. C. *Acta Crystallogr.* **1950**, *3*, 245. (b) Mason, R. *Acta Crystallogr.* **1964**, *17*, 547.